Nonequilibrium electron dynamics in noble metals

N. Del Fatti, C. Voisin, M. Achermann, S. Tzortzakis, D. Christofilos, and F. Vallée
Laboratoire d'Optique Quantique du CNRS, Ecole Polytechnique, 91128 Palaiseau cedex, France
(Received 8 February 2000)

Electron-electron and electron-lattice interactions in noble metals are discussed in the light of two-color femtosecond pump-probe measurements in silver films. The internal thermalization of a nonequilibrium electron distribution created by intraband absorption of a pump pulse is followed by probing the induced optical property changes in the vicinity of the frequency threshold for the *d* band to Fermi surface transitions. This is shown to take place with a characteristic time constant of 350 fs, significantly shorter than previously reported in gold. This difference is ascribed to a weaker screening of the electron-electron interaction by the *d*-band electrons in silver than in gold. These results are in quantitative agreement with numerical simulations of the electron relaxation dynamics using a reduced static screening of the electron-electron Coulomb interaction, and including bound electron screening. Electron-lattice thermalization has been studied using a probe frequency out of resonance with the interband transitions. In both materials, the transient nonthermal nature of the electron distribution leads to the observation of a short-time delay reduction of the energy-loss rate of the electron gas to the lattice, in very good agreement with our theoretical model.

I. INTRODUCTION

The interaction processes of conduction-band electrons between themselves and with their environment play a key role in the fundamental properties of metallic systems. They have been extensively investigated in quasiequilibrium situations using cw techniques that, however, only give global information on the electron scattering.[1,2] With the advance of femtosecond lasers, the different elementary scattering mechanisms can now be selectively addressed using time-resolved techniques. These are based on selective electron excitation on a time scale shorter than that of electron-electron and/or electron-lattice energy redistribution. The nonequilibrium electron relaxation is then followed by a probe pulse monitoring an electron-distribution-dependent property of the metal sample, such as its optical response[3–10] or the induced photoelectron emission.[11–18] Properly choosing the probing conditions and pulse durations, different mechanisms can be investigated, and information has been obtained, for instance, on electron-phonon coupling,[5–9] electron-electron scattering,[6,7,11–18] electron-spin relaxation,[19,20] and electronic transport.[21,22]

In noble metals, it was demonstrated either directly, using time-resolved two-photon photoemission[11–18] or femtosecond optical property modulation,[6] or indirectly, investigating electron-phonon interactions,[7,9,23] that internal thermalization of the conduction electrons (i.e., establishment of an electronic temperature) takes place on a time scale of a few hundred femtoseconds. The photoemission technique has the main advantage of yielding information on the energy dependence of the electron-scattering time, but with a limited precision on its absolute value and a complicated signal interpretation due to simultaneous depopulation and repopulation (cascade) effects.[13,18] Similar information can in principle be obtained by measuring the optical property changes in a large probe frequency range, provided that the metal sample band structure is known over a large energy range. Investigations have thus been limited to a few probe frequency regions, either in or out of resonance with the interband transitions, permitting a selective analysis of the energy redistribution processes both in the electron gas and to the lattice. The obtained information is more global, but permits a precise determination of the characteristic thermalization times that can thus be quantitatively compared to the prediction of a theoretical modeling of the electron interactions.

In particular, creating an athermal electron distribution by a pump pulse, and probing the induced sample transmissivity or reflectivity changes around the threshold for the *d*-band to Fermi-surface transitions, the time behavior of the electron occupation around the Fermi energy can be followed. This permits one to study the internal thermalization dynamics of the electron gas and thus the electron-electron interactions. Such investigations have only been performed in gold film,[6] and here we use a similar approach for studying electron-gas internal thermalization in silver. The properties of the conduction electrons being similar in the two metals, the measured dynamics can be compared and interpreted using a similar theoretical approach. Our modeling of the electron relaxation dynamics is based on a numerical resolution of the Boltzmann equation with a reduced static screening of the electron-electron Coulomb interactions (Sec. II). The results are compared to the experimental ones in silver, and to those previously reported in gold both for weak and strong perturbations of the electron gas,[6,24] and to the electron-scattering times measured in silver by other techniques (Sec. IV).

The short-time-scale athermal character of the electron distribution leads to a transient reduction of the electron-gas–lattice energy exchanges that have been studied performing femtosecond experiments with a probe pulse out of resonance with the interband transitions.[7,9] Extension of these measurements to both gold and silver films is discussed in Sec. V, and the results are compared quantitatively to the ones obtained using our theoretical model.

II. THEORETICAL MODEL

After ultrafast energy injection in the conduction electrons by a femtosecond pulse, the energy is redistributed among the electrons by electron-electron (e-e) scattering (internal thermalization), and transferred to the lattice by electron-phonon (e-ph) interaction (external thermalization). The relaxation dynamics can be modeled using the quasiparticle approach of the Fermi-liquid theory and describing the conduction-electron system by a one-particle distribution function f. Its time evolution is given by the Boltzmann equation

$$\frac{df(\mathbf{k})}{dt}=\left.\frac{df(\mathbf{k})}{dt}\right|_{e\text{-}e}+\left.\frac{df(\mathbf{k})}{dt}\right|_{e\text{-}ph}+H(\mathbf{k},t), \tag{1}$$

where $f(\mathbf{k})$ is the occupation number of the $\mathbf{k}$ electron-state, and $H(\mathbf{k},t)$ stands for electron-gas excitation by the pump pulse.

The electron-electron scattering rate can be written as the sum of two terms describing scattering in and out of the $\mathbf{k}$ state, respectively:

$$\left.\frac{df(\mathbf{k})}{dt}\right|_{e-e}=[1-f(\mathbf{k})]S_e^+(\mathbf{k})+f(\mathbf{k})S_e^-(\mathbf{k}), \tag{2}$$

where the scattering probabilities S_e^+ and S_e^- include both normal and umklapp electron-electron-scattering processes.[25] Calculation of the latter is too computer time consuming to be included in electron kinetic simulations; and although they can significantly contribute,[26] they will be neglected here. $S_e^{\pm}$ is then given by

$$S_e^{\pm}(\mathbf{k})=\frac{2\pi}{\hbar}\sum_{\mathbf{k}_1,\mathbf{k}_2,\mathbf{k}_3}|M(\mathbf{k},\mathbf{k}_1,\mathbf{k}_2,\mathbf{k}_3)|^2\left[\frac{1}{2}\pm\frac{1}{2}-f(\mathbf{k}_1)\right]\times\left[\frac{1}{2}\mp\frac{1}{2}-f(\mathbf{k}_2)\right]\left[\frac{1}{2}\mp\frac{1}{2}-f(\mathbf{k}_3)\right]\delta_{\mathbf{k}}\delta_E. \tag{3}$$

$\delta_{\mathbf{k}}$ and δ_E stand for momentum and energy conservations: $\mathbf{k}+\mathbf{k}_1-\mathbf{k}_2-\mathbf{k}_3=0$ and $E(\mathbf{k})+E(\mathbf{k}_1)-E(\mathbf{k}_2)-E(\mathbf{k}_3)=0$. The quasiparticle interactions are described by a screened Coulomb potential and, neglecting the exchange term, the scattering amplitude reads

$$|M|^2=\frac{e^4}{q^4\varepsilon_0^2|\varepsilon[\mathbf{q},E_{ex}]|^2}, \tag{4}$$

where the dielectric constant ε is a function of both the momentum $\mathbf{q}=\mathbf{k}-\mathbf{k_2}$ and energy $E_{ex}=E(\mathbf{k})-E(\mathbf{k_2})$ exchanged during the collision. Calculation of the screening factor $1/|\varepsilon|^2$ is a key problem in modeling e-e interaction. Using the self-consistent-field method or, equivalently, the random-phase approximation, ε has been shown to be well described by Lindhard's expression[25]

$$\varepsilon(\mathbf{q},E_{ex})=\varepsilon_b^0+\frac{e^2}{\varepsilon_0 q^2}\sum_{\mathbf{q}'}\frac{f(\mathbf{q}')-f(\mathbf{q}-\mathbf{q}')}{E(\mathbf{q}-\mathbf{q}')-E(\mathbf{q}')-E_{ex}+i\hbar\gamma}. \tag{5}$$

The first term ε_b^0 is due to screening by the core electrons, and is dominated by the d-band electron contribution in noble metals. The energy exchanged during an e-e collision always being much smaller than the interband transition energy threshold, the ε_b^0 dispersion can be neglected. As a first approximation, we have also neglected its $\mathbf{q}$ dependence, and identified it with its long-wavelength static value $\varepsilon_b(0,0)=\varepsilon_b^0$. This has been estimated from the tabulated refractive indexes,[27] following the procedure of Ehrenreich and Philipp[28,29] (Table I).

TABLE I. Fermi energy E_F (Ref. 32), conduction electron mass m (Refs. 28, 32, and 36), static interband dielectric function ε_b^0 (Ref. 29) and Debye temperature Θ_D (Ref. 32) for silver and gold. $\beta=q_S/q_{TF}$ is the screening reduction factor, Ξ is the effective deformation potential deduced from fitting the experimental results, and g is the corresponding effective electron-phonon coupling constant [Eq. (16)].

	E_F (eV)	m/m_0	ε_b^0	β	Θ_D (K)	Ξ (eV)	g (W/Km^3)
Ag	5.49	1	3.7	0.73	215	2.9	2.3×10^{16}
Au	5.53	1	6.7	0.73	170	3.7	2×10^{16}

The second term in Eq. (5) describes screening by the conduction electrons. Its expression is too complicated to be directly inserted into numerical simulations and, as usually done, we have approximated it by its static limit for small q, yielding

$$\varepsilon(\mathbf{q},E_{ex})\approx\varepsilon(q,0)=\varepsilon_b^0\left(1+\frac{q_S^2}{q^2}\right), \tag{6}$$

where q_S is identical to the Thomas-Fermi wave vector q_{TF}:

$$q_{TF}^2=\frac{e^2}{\varepsilon_0\varepsilon_b^0}\sum_{\mathbf{k}}\frac{\partial f}{\partial E}. \tag{7}$$

The Thomas-Fermi expression [Eq. (6)] yields a good approximation of Lindhard's expression if E_{ex} is small as compared to the plasmon energy.[30] This is the case in our conditions where the maximum energy that can be efficiently exchanged during a collision is the maximum nonequilibrium electron energy relative to E_F (i.e., the pump photon energy for intraband excitation). The screening factors computed using Eqs. (5) and (6) for an isotropic parabolic conduction band are compared in Fig. 1. The Thomas-Fermi expression reproduces well the q dependence of ε,[31] but overestimates its absolute value and thus the effect of screening. We have thus used the screening wave vector q_S as an adjustable parameter, defining $q_S=\beta q_{TF}$, where β (<1) is set by fitting the experimental results.

The conduction band of the noble metals around the Fermi level is well described by an isotropic free-electron model.[32] f then only depends on the electron energy, greatly simplifying the theoretical description of the energy redistribution processes. Using standard calculation, the e-e scattering rate can be transformed into an energy-dependent expression[33,34]

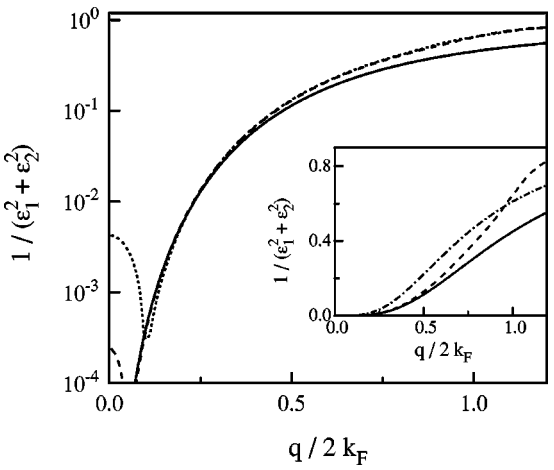

FIG. 1. Wave-vector dependence of the screening factor $1/|\varepsilon(q,E_{ex})|^2$ calculated using Lindhard's expression for $E_{ex}/4E_F=0.05$ (dashed line) and 0.1 (dotted line), and in the Thomas-Fermi approximation (full line) for $\varepsilon_b^0=1$. The inset shows the same data (except for $E_{ex}/4E_F=0.1$) on a linear scale, together with that for a reduced static screening [Eq. (6)], with $\beta=0.73$ (dash-dotted line).

$$\left.\frac{df(E)}{dt}\right|_{e-e}=\frac{me^4}{32\pi^3\hbar^3(\varepsilon_0\varepsilon_b^0)^2E_S\sqrt{E}}\int\int dE_1dE_2 \times\left[\frac{\sqrt{\tilde{E}}}{\tilde{E}+E_S}+\frac{1}{\sqrt{E_S}}\arctan\sqrt{\frac{\tilde{E}}{E_S}}\right]_{\tilde{E}_{min}}^{\tilde{E}_{max}} \times\{[1-f(E)][1-f(E_1)]f(E_2)f(E_3) -f(E)f(E_1)[1-f(E_2)][1-f(E_3)]\}, \quad (8)$$

where $E_S=\hbar^2q_S^2/2m$. The limits reflect energy and momentum conservations, and are defined by

$$\tilde{E}_{max}=\inf\{(\sqrt{E_1}+\sqrt{E_3})^2;\ (\sqrt{E}+\sqrt{E_2})^2\},$$
$$\tilde{E}_{min}=\sup\{(\sqrt{E_1}-\sqrt{E_3})^2;\ (\sqrt{E}-\sqrt{E_2})^2\}. \quad (9)$$

Note that taking into account only scattering out of the E state [Eqs. (2) and (3)] and assuming a Fermi-Dirac distribution at zero temperature, one obtains the usual expression for the electron lifetime in the vicinity of the Fermi surface due to inelastic e-e collisions:[33,17]

$$\frac{1}{\tau_{e\text{-}e}(E)}=\frac{me^4(E-E_F)^2}{64\pi^3\hbar^3\varepsilon_0^2(\varepsilon_b^0)^2E_S^{3/2}\sqrt{E_F}} \times\left[\frac{2\sqrt{E_FE_S}}{4E_F+E_S}+\arctan\sqrt{\frac{4E_F}{E_S}}\right]. \quad (10)$$

In our previous simulations the e-ph interactions were introduced in the relaxation-time approximation.[6] Although a good description of the experimental results has been obtained, the short-time-scale features associated with the interaction of a nonequilibrium electron gas with the lattice are overlooked, since a constant energy-transfer rate is implicitly assumed.[9] Here we have introduced e-ph interaction, assuming deformation potential coupling. Although it is a rough approximation in metal,[35] it turns out that the type of coupling (and the associated wave-vector dependence of the scattering matrix elements) does not influence the computed dynamics, as long as the e-ph interaction amplitude is used as a parameter set by reproducing the energy transfer rate measured for long delays. This is due to the fact that, since the lattice temperature T_L is larger than the Debye temperature, electron distribution changes on the energy scale of a phonon have a minor influence on the overall dynamics.

Neglecting umklapp processes, the e-ph scattering rate can be readily calculated for an isotropic phonon band:

$$\left.\frac{df(E)}{dt}\right|_{e-ph}=\frac{\Xi^2\sqrt{m}}{4\pi\rho\sqrt{2E}}\int_0^{q_D}dq\,\frac{q^3}{E_q}\{[1-f(E)][f(E-E_q)n_q +f(E+E_q)(1+n_q)]-f(E)\{[1-f(E-E_q)] \times(1+n_q)+[1-f(E+E_q)]n_q\}\}, \quad (11)$$

where ρ is the material density and n_q the occupation number of the q phonon with energy E_q. Ξ is the effective deformation potential constant which is used as an adjustable parameter to fit the experimental data. In the following, the Debye model will be used but, as for the coupling mechanism, the results were found to be insensitive to the phonon band structure (i.e., Debye, Einstein or sine), except for a change of Ξ.

In our experiments the electrons are driven out of equilibrium by intraband absorption of a femtosecond pump pulse of frequency ω_{pp}. This leads to the creation of an athermal distribution where electrons with an energy E between $E_F-\hbar\omega_{pp}$ and E_F are excited above the Fermi energy, with a final energy between E_F and $E_F+\hbar\omega_{pp}$ (Fig. 2). In an optically thin sample, the excitation inhomogeneity along the pump beam propagation direction can be neglected and the excitation function $H(\mathbf{k},t)$ be written

$$H(\mathbf{k},t)=H(E,t)=AI_p(t)\{\sqrt{E-\hbar\omega_{pp}}f(E-\hbar\omega_{pp}) \times[1-f(E)]-\sqrt{E+\hbar\omega_{pp}}f(E) \times[1-f(E+\hbar\omega_{pp})]\}, \quad (12)$$

where $I_p(t)$ is the pump pulse intensity, and A a constant.

The electron distribution change Δf, computed using Eqs. (1), (8), (11), and (12) for excitation of an Ag film by a 25-fs near-infrared ($\hbar\omega_{pp}=1.45$ eV) pulse, is shown in Fig. 2 for time delays of 0 (maximum of the pump pulse), 100, and 400 fs (the metal characteristics used in the simulations are given in Table I). It initially extends over a very broad range, and subsequently strongly narrows as the electron-gas internally thermalizes, the perturbed zone being then limited to a region of the order of k_BT_e around E_F (where T_e is the electron-gas temperature).

Electron distribution changes induce alterations of the optical property that are detected experimentally. In the perturbative regime, the differential transmission $\Delta T/T$ and reflection $\Delta R/R$ at a probe frequency ω_{pr} are linear combinations of the changes of the real and imaginary parts of the optical dielectric function:

$$\Delta T/T(\omega_{pr})=t_1\Delta\varepsilon_1(\omega_{pr})+t_2\Delta\varepsilon_2(\omega_{pr}),$$
$$\Delta R/R(\omega_{pr})=r_1\Delta\varepsilon_1(\omega_{pr})+r_2\Delta\varepsilon_2(\omega_{pr}), \quad (13)$$

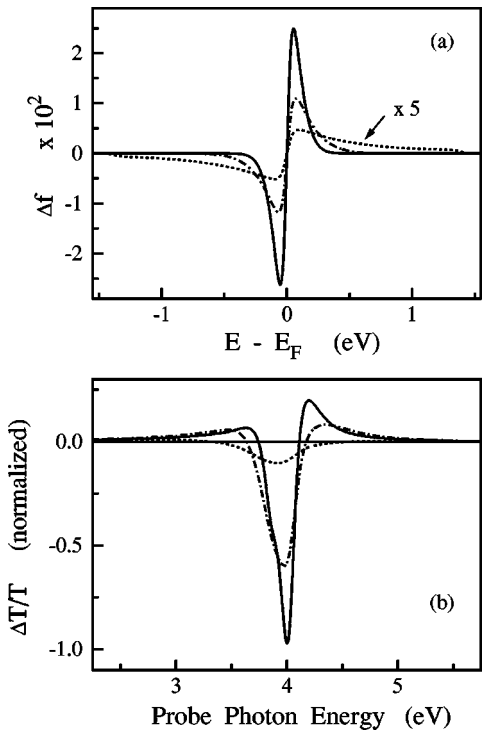

FIG. 2. (a) Computed electron distribution change in silver induced by intraband absorption of a 25-fs pulse ($\hbar\omega_{pp}=1.34$ eV), for time delays of 0 fs (dotted line), 100 fs (dash-dotted line), and 400 fs (full line) and $\Delta T_e^{me}=100$ K. (b) Corresponding computed transmission changes $\Delta T/T$ for a 23-nm-thick film.

where the coefficients t_1, t_2, r_1, and r_2 are also ω_{pr} dependent. They have been computed from the equilibrium dielectric function,[36] taking into account the Fabry-Perot effect in optically thin films.[37]

To compare the experimental and theoretical results, $\Delta\varepsilon_1$ and $\Delta\varepsilon_2$ have to be connected to Δf. Using Lindhard's expression [Eq. (5)] for $\mathbf{q}=\mathbf{0}$, including the electron optical scattering rate γ,[38] one obtains the usual expression for ε,

$$\varepsilon(\omega)=\varepsilon^{ib}(\omega)-\frac{\omega_p^2}{\omega(\omega+i\gamma)}, \tag{14}$$

where ω_p is the plasma frequency. In noble metals, for frequencies around the interband transition threshold Ω_{ib} (with $\hbar\Omega_{ib}\approx 4.1$ eV in silver), the interband term ε^{ib} is dominated by transitions from the upper d band to the Fermi surface in the vicinity of the L point of the Brillouin zone. The change of ε^{ib} can be related to Δf using the L-point band-structure models developed by Rosei and co-workers for interpreting cw thermomodulation measurements in silver and gold films.[39,40] The $\Delta T/T$ dispersion computed in silver using this approach is shown in Fig. 2(b). $|\Delta T/T|$ exhibits a large amplitude around $\hbar\omega_{pr}=4$ eV with a delayed maximum value, reflecting the strong rise of $|\Delta f|$ around E_F as the electron gas reaches a Fermi distribution [Fig. 2(a)].

A change of the electron distribution also induces a modification of the efficiency of the different electron-scattering processes entering γ, and thus of the intraband part of ε [Eq. (14)]. These changes are related to a weakening of the effect of the Pauli exclusion principle, and have been computed in the thermalized regime.[1] Extension of these calculations to the nonequilibrium regime, including the electron dynamics, is a complex many-body problem, and is beyond the scope of this paper, where we are mostly dealing with features associated with $\Delta\varepsilon^{ib}$.

III. EXPERIMENTAL SYSTEM

Measurements were performed in optically thin silver (23 nm) and gold (25 nm) polycrystalline films. The experimental setup is based on a femtosecond Ti:sapphire oscillator, generating 25-fs-frequency tunable near-infrared pulses with an average power of 1 W at 80 MHz. Part of the pulse train is used as the pump beam, and induced transmissivity $\Delta T/T$ and reflectivity $\Delta R/R$ changes are measured using a probe pulse either out or in resonance with the interband transitions. The interband transition thresholds in silver and gold being $\hbar\Omega_{ib}\approx 4.1$ eV and ≈ 2.4 eV, respectively, off-resonant condition can be realized using a near-infrared probe at the same frequency as the pump pulse or, in silver, at its second harmonic.

To probe the interband transitions in silver, we have generated femtosecond UV pulses by frequency tripling the Ti:sapphire oscillator pulses. Part of the pulse train was first frequency doubled in a 100-μm-thick BBO (beta barium borate) crystal, and the infrared ω_{IR} and blue ω_B pulses were subsequently independently recompressed in fused silica prism pairs. The UV pulses were then created performing the sum frequency $\omega_{IR}+\omega_B$ in a second 100-μm-thick BBO crystal and temporally recompressed in a prism pair. The typical UV average power was 10 μW. Cross-correlation of the IR pump and UV probe pulses was measured at the position of the sample by difference frequency mixing in a BBO crystal, yielding an UV pulse duration of about 60 fs.

For all the probe wavelengths, a standard pump-probe setup has been used, with a mechanical chopping of the pump beam and lock-in detection of the probe beam transmission or reflection changes. The pump and probe beams were independently focused into the sample using fused silica lenses of 50- and 70-mm focal lengths, respectively. The high repetition rate (80 MHz) and stability of our femtosecond system permits noise levels for $\Delta T/T$ and $\Delta R/R$ measurements in the 10^{-6} range, and thus investigations in the low-perturbation regime (pump fluences in the 5–200 μJ/cm^{-2} range). It is convenient to characterize the energy injected by the pump pulse by defining a maximum equivalent electron temperature rise ΔT_e^{me} as the temperature increase of a thermalized electron gas for the same injected energy. Using the measured pump pulse absorption and the electronic heat capacity of silver ($\sim 65\times T_e$ Jm^{-3}K^{-1}), ΔT_e^{me} ranges from 2 to 80 K. The electron heat capacity C_e being much smaller than the lattice one C_L, the final temperature rise of the fully thermalized electron-lattice system is always smaller than 0.7 K.

IV. INTERNAL ELECTRON-GAS THERMALIZATION

A. Optical investigation: Low-perturbation regime

The temporal evolution of the induced differential transmissivity $\Delta T/T$ measured in the silver film is shown in Fig. 3 for different probe photon energies $\hbar\omega_{pr}$ around $\hbar\Omega_{ib}$. The maximum $|\Delta T/T|$ amplitude is observed around $\hbar\omega_{pr}^M$

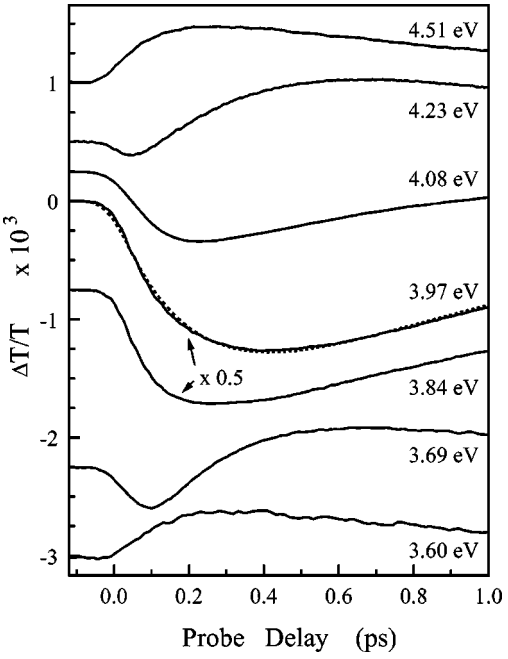

FIG. 3. Measured time dependence of the differential transmission $\Delta T/T$ in a 23-nm-thick silver film for different probe photon energies around $\hbar\Omega_{ib}$ and $\Delta T_e^{me}\approx 18$ K. The different curves are vertically displaced for clarity. The dashed line is a phenomenological fit assuming an exponential signal rise and decay [Eq. (15)].

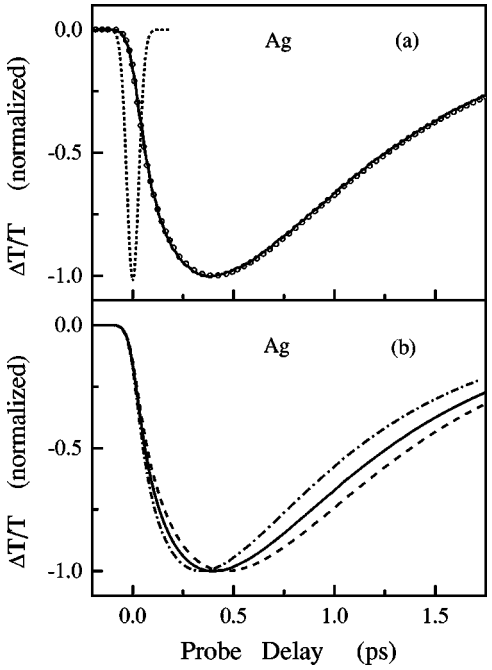

FIG. 4. (a) Differential transmission $\Delta T/T$ measured (full line) and computed (for $\beta=0.73$, open dots) at $\hbar\omega_{pr}=3.97$ eV in a 23-nm silver film for $\Delta T_e^{me}\approx 50$ K. The dotted line is the pump-probe cross-correlation. (b) Computed $\Delta T/T$ at $\hbar\omega_{pr}=4$ eV for $\beta=0.63$ (dash-dotted line), 0.73 (full line), and 0.83 (dashed line).

$=4$ eV, with $\Delta T/T<0$, in good agreement with the cw thermotransmission measurements[41] and the theoretical modeling of Sec. II. The dependence of the $\Delta T/T$ temporal shape on $\hbar\omega_{pr}$ is similar to that reported in gold films[6] with, in particular, the same change of sign of $\Delta T/T$ with time when probing away from $\hbar\omega_{pr}^{M}$ [Fig. 2(b)]. This complex behavior is a signature of the delayed internal thermalization of the nonequilibrium electron gas, and was discussed in detail in Ref. 6. A similar analysis can be performed for silver, and thus will not be repeated here. We will focus on the time behavior of $\Delta T/T$ around $\hbar\omega_{pr}^{M}$ which contains quantitative information about the internal thermalization dynamics of the electron gas.

The measured $\Delta T/T$ is shown in more detail in Fig. 4(a) for $\hbar\omega_{pr}\approx 3.97$ eV and $\Delta T_e^{me}\approx 50$ K. Similar behaviors were observed for ΔT_e^{me} in the range 80–2 K. $\Delta T/T$ reaches its maximum value after only ~ 400 fs, and subsequently decays due to electron-lattice energy transfer. This delayed rise reflects the finite buildup time of the change of occupation number of the probed electron states around E_F, and is thus a measure of the electron-gas internal thermalization dynamics.

A characteristic internal thermalization time τ_{th} can be defined by assuming a monoexponential signal rise, and fitting the experiments with a response function of the form

$$R(t)=H(t)\{A[1-\exp(-t/\tau_{th})]\exp(-t/\tau_{e\text{-}ph}) + B[1-\exp(-t/\tau_{e\text{-}ph})]\}, \quad (15)$$

where $H(t)$ is the Heaviside function. The first term describes the purely electronic response which rises with the time constant τ_{th} and decays by energy transfer to the lattice with the effective electron-phonon coupling time $\tau_{e\text{-}ph}\approx 850$ fs. The second term accounts for the small residual signal ($B\ll A$) due to the weak heating of the lattice, and thus rises with $\tau_{e\text{-}ph}$. A good reproduction of the $\Delta T/T$ behavior is obtained by convolving the pump-probe cross correlation with R using $\tau_{th}=\tau_{th}^{Ag}\approx 350$ fs (Fig. 3). Probing around $\hbar\Omega_{ib}$, only the distribution change around E_F is detected, and although τ_{th} *a priori* reflects electron redistribution over the full excited region, it is actually essentially determined by *e-e* collisions around the Fermi surface [Fig. 2(a)]. Their probability being largely reduced by Pauli exclusion principle effects, they are the slowest scattering processes involved in the internal thermalization and thus lead to the observed long τ_{th}.

The internal thermalization time in silver is significantly shorter than the one measured in gold: $\tau_{th}^{Au}\approx 500$ fs.[6] The conduction-electron properties being similar in the two metals, this difference can be ascribed to weaker screening by the bound electrons in Ag (Table I). The *e-e* scattering efficiency being roughly proportional to $1/\sqrt{\varepsilon_b^0}$ [Eq. (10)], τ_{th} is expected to be about 35% larger in gold than in silver ($\tau_{th}^{Au}/\tau_{th}^{Ag}\approx 1.35$), in agreement with the experimental result: $\tau_{th}^{Au}/\tau_{th}^{Ag}\approx 1.4$.

A more precise description of the transient $\Delta T/T$ measured in silver can be obtained by comparing it to the one computed with the model of Sec. II. Using static screening with $\beta=1$, the temporal shape is qualitatively reproduced, with the results showing, as expected, a rise time essentially determined by the *e-e* interactions and a decay time by the *e*-ph coupling. A much slower rise time is however computed, indicating underestimation of the *e-e* scattering efficiency consistent with screening overestimation in the static approximation [Fig. (1)]. A quantitative reproduction of the

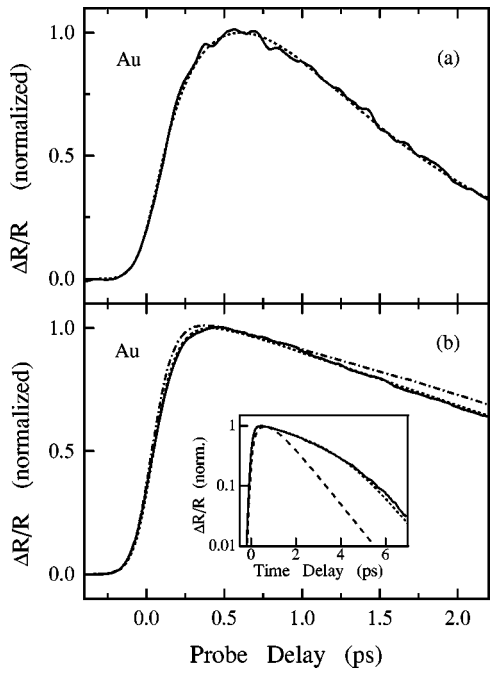

FIG. 5. (a) Measured differential reflectivity $\Delta R/R$ for $\hbar\omega_{pr}=2.5$ eV in a 20-nm-thick gold film for $\Delta T_e^{me}\approx 15$ K (full line, from Ref. 6). The dotted line is the computed $\Delta R/R$ for $\beta=0.73$. (b) Measured $\Delta R/R$ for $\Delta T_e^{me}\approx 1300$ K (full line, from Ref. 40). The dash-dotted and dotted lines are computed for $\Delta T_e^{me}=1300$ and 1100 K, respectively. The inset shows the same results on a semilogarithmic scale, together with the computed $\Delta R/R$ for $\Delta T_e^{me}=100$ K (dashed line).

data is obtained using a reduced screening with $\beta=0.73$ [Fig. 4(a)], which corresponds to renormalizing the static screening term to better match Lindhard's expression over the range of exchanged wave vectors (inset of Fig. 1). However, it has to be noted that β also phenomenologically compensates for the various approximations performed in modeling e-e scattering, in the Born approximations and neglecting exchange effects and umklapp processes.[25] The second parameter entering the model, i.e., the effective e-ph deformation potential Ξ, is given in Table I, and is consistent with its value for a free-electron gas [$\Xi^f=2/3E_F\approx 3.7$ eV (Ref. 32)]. As Ξ is independently determined by the long-time-scale signal decay, the short-time delay behavior is mainly determined by β and is very sensitive to its value. This is illustrated in Fig. 4(b), displaying the time dependence of $\Delta T/T$ at $\hbar\omega_{pr}^M$ computed for $\beta=0.63$, 0.73, and 0.83.

The conduction-band properties of gold and silver being similar (Table I), the same electron kinetic model can be used to analyze the results of Sun *et al.* in gold.[6] Using Rosei *et al.*'s band structure model for gold,[40] the transient differential reflectivity measured around its maximum amplitude ($\hbar\omega_{pr}^M\approx 2.5$ eV) is quantitatively reproduced using the same screening reduction factor $\beta=0.73$,[42] the only remaining free parameter here being the effective e-ph coupling [Fig. 5(a)]. The same agreement is obtained for the transmissivity change. The different electron thermalization time measured in gold and silver can thus be entirely ascribed to the larger d-band electron screening in gold.

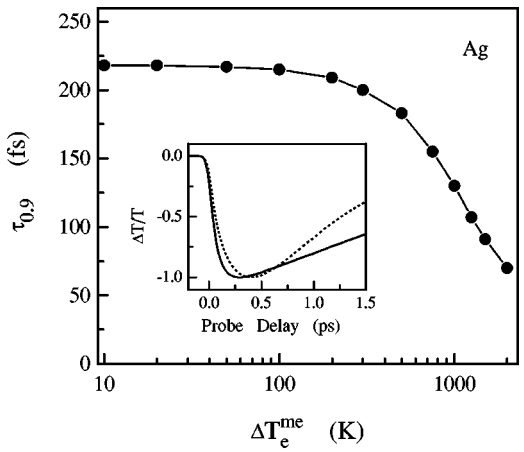

FIG. 6. Computed time delay $\tau_{0.9}$ for which $|\Delta T/T|$ has reached 90% of its maximum value at $\hbar\omega_{pr}=4$ eV in silver as a function of the energy injected in the electron gas measured by ΔT_e^{me}. The inset shows $\Delta T/T$ computed for $\Delta T_e^{me}=100$ K (dotted line) and 1000 K (full line).

B. Optical investigation: Strong-perturbation regime

The above investigation has been performed in the low-perturbation regime, i.e., for typically $\Delta T_e^{me}\leqslant 200$ K, for which nonequilibrium electron relaxation is essentially determined by the unperturbed electron properties, and is thus almost independent of the incident pump power. For larger energy injection, the impact of the induced electron distribution change on the scattering rates becomes significant leading to pump-power-dependent temporal shape of the measured signals.[5,24]

The reflectivity change $\Delta R/R$ measured by Sun *et al.* in a 20-nm-thick gold film for $\Delta T_e^{me}=1300$ K at $\hbar\omega_{pr}\approx 2.5$ eV is shown in Fig. 5(b). It exhibits a faster rise time and a longer decay time than for low perturbation [$\Delta T_e^{me}=15$ K, Fig. 5(a)]. $\Delta R/R$, calculated using the β and Ξ values determined in Sec. IV A (Table I), shows the same type of behavior, though with a slightly faster rise and a slower decay than the experimental ones [Fig. 5(b)], indicating an overestimation of ΔT_e^{me}. A quantitative agreement is obtained for both the signal decay and rise times using a slightly reduced value $\Delta T_e^{me}=1100$ K in the simulations. This difference is likely due to an overestimation of the film absorption and/or to the averaging effect due to the electron temperature gradient over the probed region, as a consequence of the spatial pump intensity profile.

The signal rise time decrease with increasing the perturbation can be related to the large induced smearing of the electron distribution around the Fermi energy and to the concomitant increase of the e-e scattering efficiency due to weakening of the effects of the Pauli exclusion. A significant acceleration of the electron internal thermalization takes place for ΔT_e^{me}, typically larger than 300 K, as shown in Fig. 6 for silver, where the calculated delay for which $|\Delta T/T|$ has reached 90% of its maximum value has been plotted as a function of ΔT_e^{me} (this only represents a crude estimation of the thermalization dynamics since the signal decay time is also changing; see the inset of Fig. 6).

The concomitant slowing down of the electron gas cooling is also very well reproduced by the simulations, and is a

consequence of the temperature dependence of the electron heat capacity.[5] After internal thermalization, the electron distribution is entirely described by its temperature T_e (i.e., its total energy), and thus its dynamics by the T_e dynamics. This can be described by computing the energy-loss rate to the lattice using the Boltzmann equation [Eq. (1)], leading to the well-known rate-equation system of the two-temperature model:[43]

$$C_e(T_e)\partial T_e/\partial t = -g(T_e - T_L),$$
$$C_L \partial T_L/\partial t = g(T_e - T_L), \tag{16}$$

where T_L is the lattice temperature. The effective electron-phonon coupling constant g is related to Ξ by

$$g = \frac{k_B m^2 q_D^4 \Xi^2}{16\rho\pi^3\hbar^3}. \tag{17}$$

For a weak perturbation, i.e., $T_e - T_0 \ll T_0$, $C_e(T_e) = \gamma T_e$ can be identified with $C_e(T_0)$ leading to an exponential decay of the electron temperature with the time constant $\tau_{e\text{-}ph} \approx \gamma T_0/g$, in agreement with the experimental results.[24]

In contrast, for large perturbations, a nonexponential behavior is obtained, with a large slowing down of the T_e short-time delay decrease, which is eventually followed by an exponential decay with the time constant $\tau_{e\text{-}ph}$ as T_e approaches T_L. This behavior is in agreement with the measured one, and with that computed using the general approach of Sec. II [see the inset of Fig. 5(b)]. However in this nonlinear regime, extraction of the *e*-ph coupling constant or of an internal thermalization time is difficult, the observed behavior depending strongly on the energy injected into the electron gas.

C. Comparison with other measurements

Time-resolved two-photon photoemission has been extensively used to study electron relaxation in noble metals.[11–18] In these experiments, the dynamics of conduction-electron states excited by a femtosecond pulse is followed as a function of their energy by monitoring the number and energy of electrons photoemitted by a delayed probe pulse. The precision of the results is limited by the difficulty in determining the absolute relaxation time and electron energy, only their relative variations being precisely obtained (Fig. 7). In the case of silver, only intraband excitation takes place, and the experiments can be described using the model of Sec. II. Following the experimental approach, an effective electron relaxation time τ_{phot} is defined by fitting the signal calculated for an equal-pulse correlation configuration, assuming a monoexponential system response.[14] Although no parameter is used here, the times calculated for a reduced screening with $\beta = 0.73$ are in good agreement with the measured ones while $\beta = 1$ leads to a large overestimation of τ_{phot} (Fig. 7).

τ_{phot} is essentially determined by *e*-*e* collisions, but is significantly larger than the scattering time $\tau_{e\text{-}e}^{out}$ of an electron out of its state by *e*-*e* collisions calculated using Eq. (8), with $\beta = 0.73$ (dashed line in Fig.7), due to repopulation of the lower-energy states during relaxation of the higher-energy electrons (cascading effect[12,14,18]). For low electron energy ($E \leqslant 0.6$ eV), this competition between electron state population decay and buildup leads to a more complex time behavior of the computed photoemission signal, with a delayed maximum. Extraction of a characteristic relaxation time is then more complex, and necessitates taking into account the coupled dynamics of the different states.[18] Direct comparison of the experimental and calculated signals is more appropriate here, and thus we have limited our τ_{phot} estimation to high-energy states. Note that for low-energy states, diffusion effects that are neglected in our calculations can also play an important role.[13,14,24,44]

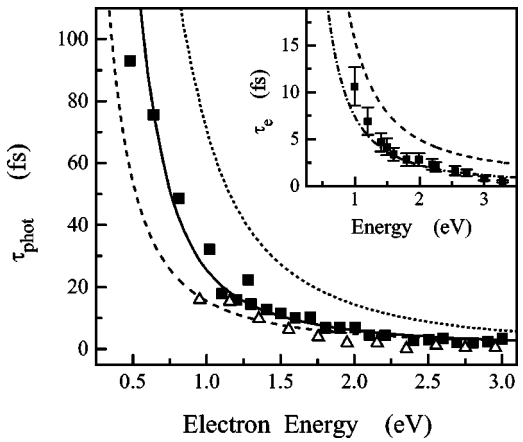

FIG. 7. Energy dependence of the electron relaxation time τ_{phot} measured by femtosecond photoemission (triangles, Ref. 13; squares, Ref. 15) and calculated with $\beta = 0.73$ (full line) and $\beta = 1$ (dotted line) in Ag. The dashed line is the electron scattering rate out of the *E* state, $\tau_{e\text{-}e}^{out}$. The inset shows the electron dephasing time τ_e measured by a space-resolved technique (squares, Ref. 44), and $\tau_{e\text{-}e}^{out}$ computed using the model of Sec. II (dashed line) and for no bound electron screening ($\varepsilon_b^0 = 1$, dash-dotted line).

Surface electron state dephasing was recently studied in silver at low temperature (5 K) using a space-resolved technique.[45] The measured dephasing times are smaller than the bulk $\tau_{e\text{-}e}^{out}$ (see the inset of Fig. 7). This suggests either pure dephasing effects (neglected in our calculations) or a surface-induced enhancement of the *e*-*e* scattering (the *e*-ph contribution is negligible). In particular, because of *d*-band electrons' exclusion from the metal surface,[46] their contribution to the screening is strongly reduced. As a rough approximation we have calculated $\tau_{e\text{-}e}^{out}$ for no *d*-band screening (i.e., for $\varepsilon_0^{ib} = 1$), which yields a much better reproduction of the data (Fig. 7). However, a more correct approach should take into account only partial *d*-band screening reduction and other surface-induced effects.[45]

V. ELECTRON-LATTICE COUPLING

On a time scale of a few hundred femtoseconds, the excited electron gas is athermal, and is thus expected to exhibit modified properties as compared to the thermal situation which is usually investigated. This can be shown by probing the transient transmissivity and reflectivity of a metal film well below Ω_{ib}. In particular, using off-resonant conditions (i.e., $\omega_{pp} + \omega_{pr} < \Omega_{ib}$), it has been shown in silver that the athermal character of the distribution leads to a slowing down of the electron gas energy losses to the lattice.[9]

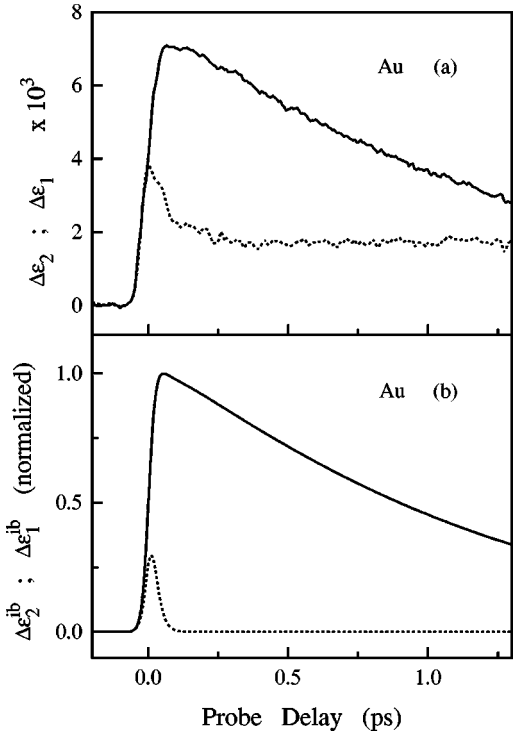

FIG. 8. (a) Measured transient changes of the real (full line) and imaginary (dotted line) parts of the dielectric function ε for $\hbar\omega_{pr}=\hbar\omega_{pp}=1.45$ eV and $\Delta T_e^{me}=55$ K in a 25-nm-thick Au film. (b) Computed changes of ε due only to its interband term.

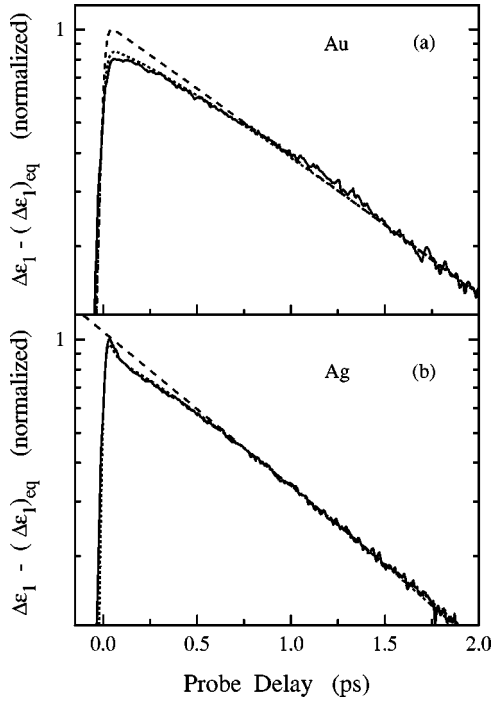

FIG. 9. (a) Measured transient change of $\Delta\varepsilon_1$ in a 25-nm Au film at $\hbar\omega_{pr}=1.45$ eV on a logarithmic scale (full line). The dotted and dashed lines are the interband contribution to $\Delta\varepsilon_1$ computed for the transient electron distribution and for a thermal electron gas, respectively. (b) Measured $\Delta\epsilon_1$ in a 23-nm Ag film for $\hbar\omega_{pr}=2.9$ eV (full line). The dashed line shows an exponential decay with $\tau_{e\text{-}ph}=850$ fs. The dotted line is the average of the calculated $\Delta\varepsilon_1$ using the Rosei and parabolic models.

We have investigated this effect in a 25-nm-thick gold film by exciting the electron gas with an infrared pulse ($\lambda_{pp}\approx 850$ nm), and probing the induced transmissivity and reflectivity changes at the same wavelength. The changes $\Delta\varepsilon_1$ and $\Delta\varepsilon_2$, deduced using Eq. (13), are shown in Fig. 8(a). The off-resonant condition being not satisfied for gold ($\hbar\omega_{pp}+\hbar\omega_{pr}>\hbar\Omega_{ib}\approx 2.4$ eV), interband absorption at ω_{pr} involves final conduction-band states around $E_e=E_F-\hbar(\Omega_{ib}-\omega_{pr})$, in the energy region where the electron occupation number is reduced during excitation (from $E_F-\hbar\omega_{pp}$ to E_F; Fig. 2). Interband absorption at ω_{pr} is thus induced, and relaxes in a few femtoseconds as short living states far from the Fermi energy are involved ($E_F-E_e\sim 0.95$ eV; the ''holes'' below E_F having a similar dynamics as the corresponding electrons above E_F, Fig. 2), leading to a fast rise and fall of $\Delta\varepsilon_2$. After this transient, $\Delta\varepsilon_2$ reaches a plateau, that can be attributed to an increase of the average electron scattering rate γ [and thus of the Drude term contribution, Eq. (14)] induced by an increase of the e-ph interaction due to the T_L rise.[9]

Using the measured $\Delta\epsilon_2$ amplitude and Eq. (14), one can easily show that the Drude contribution to $\Delta\varepsilon_1$ is negligible.[9] $\Delta\varepsilon_1$ is thus essentially due to a modification of the interband term $\Delta\varepsilon_1^{ib}$. When probing away from Ω_{ib}, $\Delta\varepsilon_1^{ib}$ is almost proportional to the excess energy ΔE_{ex} in the electron gas (i.e., the difference between its transient total energy and its quasiequilibrium one when thermalized with the lattice), and the $\Delta\varepsilon_1$ dynamics is a measure of the electron-lattice energy transfer.[9] The time evolution of $\Delta\varepsilon_1$ can be more clearly analyzed by plotting its amplitude on a logarithmic scale (Fig. 9). As in silver films, a nonexponential short-time delay behavior is observed, an exponential decay with a time constant $\tau_{e\text{-ph}}\approx 950$ fs being recovered only on a long-time scale ($t\geqslant 1$ ps). This demonstrates that the electron-gas–lattice energy-transfer rate increases with time to reach a maximum constant value when the electron gas is internally thermalized. In a simple qualitative approach, this behavior can be related to the increase of the number of electrons out of equilibrium with the lattice during redistribution of the injected energy.[7,23,47] The number of electrons that can emit a phonon and, consequently, the electron-gas energy-loss rate to the lattice, thus increases with time. This single-electron description is only valid for a strongly athermal distribution, and a constant rate is reached as the electron temperature is established, corresponding to a collective description of the electrons via their temperature [Eq. (16)].

A very good agreement with the computed transient $\Delta\varepsilon_1^{ib}$ is obtained (Fig. 9), using the model of Sec. II with, as expected, a time shape almost identical to the calculated one for ΔE_{ex}. Using the same factor to normalize the computed $\Delta\varepsilon_1^{ib}$ and $\Delta\varepsilon_2^{ib}$, the amplitude of the transient peak of the latter is also correctly reproduced [Fig. 8(b)]. The origin of the transient slowing down of the electron-gas–lattice energy transfer is confirmed by simulations performed assuming quasi-instantaneous electron thermalization (i.e., artificially increasing e-e coupling in the simulations). A monoexponential $\Delta\varepsilon_1^{ib}$ decay with the time constant $\tau_{e\text{-ph}}$ is then obtained (Fig. 9), consistent with the two-temperature model [Eq. (16)]. In addition, a negligible induced interband absorption is calculated [i.e., $\Delta\varepsilon_2^{ib}(\hbar\omega_{pr})\approx 0$], since the

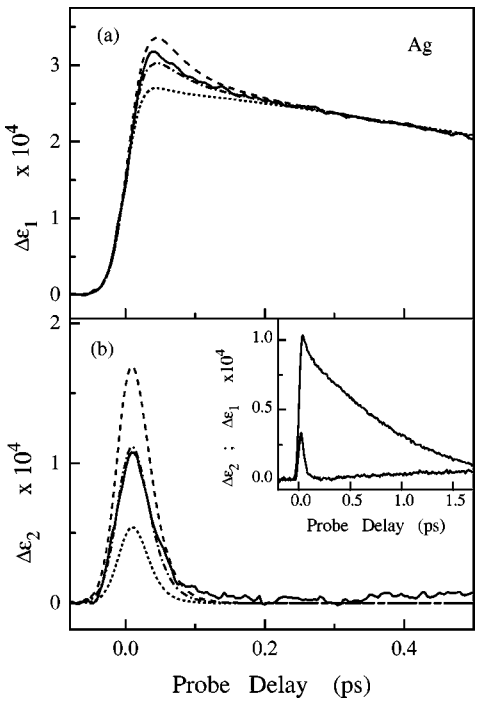

FIG. 10. Measured transient changes of the real (a) and imaginary (b) parts of the dielectric function at $\hbar\omega_{pr}=2.9$ eV in a 23-nm Ag film (full lines) for $\hbar\omega_{pp}=1.45$ eV and $\Delta T_e^{me}=18$ K; the inset shows the same results on a longer time scale. The dotted and dashed lines are the interband induced changes computed using the Rosei and parabolic band-structure models, respectively, and the dash-dotted line is their average.

changes of f are restricted to a small energy range of the order of $k_B T_e$ around E_F.

To confirm our interpretation, we have performed similar measurements in silver exciting the electron gas with an infrared pulse, and probing the transmissivity and reflectivity changes at the double frequency. The off-resonant conditions are also not satisfied here and, as expected, $\Delta\varepsilon_1$ and $\Delta\varepsilon_2$ show similar behaviors as in gold with, in contrast to our previous off-resonant study in silver,[9] a transient $\Delta\varepsilon_2$ peak due to induced interband transitions (Fig. 10). The small amplitude of the long delay $\Delta\varepsilon_2$ is consistent with the small intraband contribution to ε in the blue region of the spectrum [Eq. (14)].

Both $\Delta\varepsilon_1$ and $\Delta\varepsilon_2$ being dominated by the interband term, their experimental and theoretical time behaviors can be quantitatively compared here. The absolute amplitude of the computed $\Delta\varepsilon^{ib}$ is set by normalizing $\Delta\varepsilon_1^{ib}$ to the measured value at $t\approx 0.5$ ps, $\Delta\varepsilon_2^{ib}$ then being multiplied by the same factor. Using the band structure model of Rosei , a qualitative reproduction of the measured data is obtained, with however, a clear underestimation of the $\Delta\varepsilon_2$ amplitude as well as of the short-time delay $\Delta\varepsilon_1$ (Fig. 10). Rosei model has been developed to describe ε changes around Ω_{ib} in a quasiequilibrium regime. Only alterations of the interband transitions involving final states close to E_F thus have to be considered, and the band-structure description can be limited to the vicinity of the L point.[39] For strongly athermal distributions and probing off resonance, the induced absorption can also take place in other regions of the Brilloun zone, as states well below E_F are perturbed. This leads to a larger density of states for the transitions, and thus to a larger transient $\Delta\varepsilon_2$. To estimate the role of this effect, we have computed $\Delta\varepsilon^{ib}$, assuming undispersed d bands and a parabolic isotropic conduction band. As expected, $\Delta\varepsilon_2$ is then overestimated (Fig. 10), this model overestimating both the joint density of states for the transitions and the occupation number reduction of the final states due to neglecting d-band dispersion. A very good reproduction of both $\Delta\varepsilon_2$ and $\Delta\varepsilon_1$ is obtained by phenomenologically averaging the results obtained for the two band-structure models (Fig. 10). Note that both models yield a good qualitative description of the measured features, with a transient interband contribution to $\Delta\varepsilon_2$ and a short-time-scale nonexponential decay of $\Delta\varepsilon_1$ (Fig. 10), consistent with the results in gold and the off-resonant measurements in silver.

VI. CONCLUSION

Ultrafast electron-electron and electron-lattice interactions have been investigated in noble metals using two-color femtosecond pump-probe techniques, and modeled performing electron kinetic simulations. Experiments were performed in the low-perturbation regime in optically thin films by creating an athermal electron distribution by intraband absorption of a near-infrared pump pulse, and probing the optical property changes either in or out of resonance with the d band to conduction-band transitions. In the former case, the response is sensitive to the conduction-electron distribution around the Fermi surface, and thus to the internal thermalization of the electron gas. This is found to take place with a characteristic time $\tau_{th}\approx 350$ fs in silver, smaller than previously reported in gold $\tau_{th}\approx 500$ fs. This difference is ascribed to smaller screening of the electron-electron Coulomb interactions by the d-band electrons in silver than in gold.

The electron relaxation dynamics has been modeled by numerically solving the Boltzmann equation for quasi-free electrons. Electron-electron interactions are described using a statically screened Coulomb potential, and phenomenologically reducing the screening wave vector to take into account conduction electron screening overestimation by the Thomas-Fermi model. Electron-phonon interactions have been modeled assuming deformation potential coupling, and using a Debye model for the phonon band structure. The computed transient electron distribution are related to the optical property changes observed experimentally using the Rosei and co-workers' band-structure models.[39,40]

In both silver and gold, the computed changes are found to reproduce the experimental ones quantitatively, using the same screening reduction factor and taking into account the different d-band electron screening. The results were found to be very sensitive to the screening efficiency by both the conduction and bound electrons. The internal thermalization time τ_{th} is essentially determined by electron-electron scattering in the vicinity of the Fermi energy E_F, whose probability is strongly reduced by band-filling effects. In the low-perturbation regime (equivalent electron temperature rise $\leqslant 300$ K), the dynamics is determined by the unperturbed electron properties, and the τ_{th} decrease from gold to silver

reflects decrease of the *d*-band electron screening. For larger energy injection, the induced large smearing of the electron distribution around E_F significantly weakens the electron-electron-scattering blocking effect due to the Pauli exclusion principle. A faster electron internal thermalization is thus calculated, in very good agreement with the experimental results previously reported for gold.[24]

To test the validity of our theoretical approach, we have used it to model two-photon femtosecond photoemission experiments in silver.[14,16] The calculated effective electron relaxation times are in good agreement with the experimental ones in the electron energy range (typically $E-E_F \geqslant 0.6$ eV), where a simple fitting procedure can be used and diffusion effects neglected. The results of our model have also been compared to the surface electron dephasing times recently determined by a spatially resolved technique. The computed times have been found to be larger than the experimental ones, probably because of surface effects.

The impact of the short-time-scale athermal character of the distribution on the electron-gas–lattice energy exchanges has been studied using a probe frequency well below the interband transition threshold. The change of the real part of the dielectric function deduced from differential transmission and reflection measurements thus essentially reflects the transient excess energy in the electron gas. The results in both silver and gold films show a reduction of electron-gas energy losses to the lattice during the first few hundred femtoseconds, when the electron distribution is athermal. The transfer rate increases with time, and eventually reaches a constant value as the electron gas internally thermalizes. In both metals, the results are in quantitative agreement with our simulations and reflect the change from an individual to a collective electron behavior during electron-gas internal thermalization.

ACKNOWLEDGMENTS

The authors wish to thank M. Aeschlimann for helpful information on femtosecond photoemission measurements.

[1] M. Kaveh and N. Wiser, Adv. Phys. **33**, 257 (1984).
[2] V. A. Gasparov and R. Huguenin, Adv. Phys. **42**, 393 (1993).
[3] H. E. Elsayed-Ali, T. B. Norris, M. A. Pessot, and G. A. Mourou, Phys. Rev. Lett. **58**, 1212 (1987).
[4] R. W. Schoenlein, W. Z. Lin, J. G. Fujimoto, and G. L. Eesley, Phys. Rev. Lett. **58**, 1680 (1987).
[5] S. D. Brorson, A. Kazeroonian, J. S. Modera, D. W. Face, T. K. Cheng, E. P. Ippen, M. S. Dresselhaus, and G. Dresselhaus, Phys. Rev. Lett. **64**, 2172 (1990).
[6] C. K. Sun, F. Vallée, L. H. Acioli, E. P. Ippen, and J. G. Fujimoto, Phys. Rev. B **50**, 15 337 (1994).
[7] R. Groeneveld, R. Sprik, and A. Lagendijk, Phys. Rev. B **51**, 11 433 (1995).
[8] H. E. Elsayed-Ali, T. Juhasz, G. O. Smith, and W. E. Bron, Phys. Rev. B **43**, 4488 (1991).
[9] N. Del Fatti, R. Bouffanais, F. Vallée, and C. Flytzanis, Phys. Rev. Lett. **81**, 922 (1998).
[10] J. Hohlfeld, D. Grosenick, U. Conrad, and E. Matthias, Appl. Phys. A: Solids Surf. **60**, 137 (1995).
[11] W. S. Fann, R. Storz, H. W. K. Tom, and J. Bokor, Phys. Rev. Lett. **68**, 2834 (1992); Phys. Rev. B **6**, 13 592 (1992).
[12] A. Knoesel, A. Hotzel, T. Hertel, M. Wolf, and G. Ertl, Surf. Sci. **368**, 76 (1996).
[13] A. Knoesel, A. Hotzel, and M. Wolf, Phys. Rev. B **57**, 12 812 (1998).
[14] M. Aeschlimann, M. Bauer, and S. Pawlik, Chem. Phys. **205**, 127 (1996).
[15] M. Aeschlimann, M. Bauer, S. Pawlik, W. Weber, R. Burgermeister, D. Oberli, and H. C. Siegmann, Phys. Rev. Lett. **79**, 5158 (1997).
[16] M. Wolf and M. Aeschlimann, Phys. Bl. **54**, 145 (1998).
[17] S. Ogawa, H. Nagano, and H. Petek, Phys. Rev. B **55**, 10 869 (1997).
[18] J. Cao, Y. Cao, H. E. Elsayed-Ali, R. J. D. Miller, and D. A. Mantell, Phys. Rev. B **58**, 10 948 (1998).
[19] E. Beaurepaire, J. C. Merle, A. Daunois, and J. Y. Bigot, Phys. Rev. Lett. **76**, 4250 (1996).
[20] J. Hohlfeld, E. Matthias, R. Knorren, and K. H. Bennemann, Phys. Rev. Lett. **78**, 4861 (1997).
[21] S. D. Brorson, J. G. Fujimoto, and E. P. Ippen, Phys. Rev. Lett. **59**, 1962 (1987).
[22] C. Suarez, W.E. Bron, and T. Juhasz, Phys. Rev. Lett. **75**, 4536 (1995).
[23] G. Tas and H. J. Maris, Phys. Rev. B **49**, 15 046 (1994).
[24] C. K. Sun, F. Vallée, L. H. Acioli, E. P. Ippen, and J. G. Fujimoto, Phys. Rev. B **48**, 12 365 (1993).
[25] J. M. Ziman, *Principles of the Theory of Solids* (Cambridge University Press, Cambridge, 1969).
[26] S. L. Adler, Phys. Rev. **130**, 1654 (1963).
[27] E. D. Palik, *Handbook of Optical Constants of Solids* (Academic Press, New York, 1985).
[28] H. Ehrenreich and H. R. Philipp, Phys. Rev. **128**, 1622 (1962).
[29] Kramers-Kronig analysis was performed over larger energy ranges than in Ref. 28, leading to slightly larger ε_b^0.
[30] J. H. Collet, Phys. Rev. B **47**, 10 279 (1993).
[31] In our conditions, the maximum normalized energy is $E_N = E_{ex}/4E_F \sim 0.07$. For a fixed E_N the exchanged normalized wave vector $q/2k_F$ ranges roughly from E_N to 1.
[32] 'N. W. Ashcroft and N. D. Mermin, *Solid State Physics* (Holt-Saunders, Tokyo, 1981).
[33] D. Pines and P. Nozières, *The Theory of Quantum Liquids* (Benjamin, New York, 1966).
[34] D. W. Snoke, W. W. Rühle, Y. C. Lu, and E. Bauser, Phys. Rev. B **45**, 10 979 (1992).
[35] G. Grimvall, *The Electron-Phonon Interaction in Metals* (North-Holland, Amsterdam, 1981).
[36] P. B. Johnson and R. W. Christy, Phys. Rev. B **6**, 4370 (1972).
[37] F. Abelès, in *Advanced Optical Techniques*, edited by Van Heel (North-Holland, Amsterdam, 1967), p. 144.
[38] N. D. Mermin, Phys. Rev. B **1**, 2362 (1970).
[39] R. Rosei, Phys. Rev. B **10**, 474 (1974).
[40] R. Rosei, F. Antonangeli, and U. M. Grassano, Surf. Sci. **37**, 689 (1973).

[41] R. Rosei, C. H. Culp, and J. H. Weaver, Phys. Rev. B **10**, 484 (1974).
[42] Following Ref. 11, $\varepsilon_b^0 \approx 5.6$ was used in Ref. 6, leading to a larger value of β.
[43] M. I. Kaganov, I. M. Lifshitz, and L. V. Tanatarov, Zh. Eksp. Teor. Fiz. **31**, 232 (1957) [Sov. Phys. JETP **4**, 173 (1957)].
[44] D. Bejan and G. Raseev, Phys. Rev. B **55**, 4250 (1997).
[45] L. Bürgi, O. Jeandupeux, H. Brune, and K. Kern, Phys. Rev. Lett. **82**, 4516 (1999).
[46] A. Liebsch, Phys. Rev. Lett. **71**, 145 (1993).
[47] V. E. Gusev and O. B. Wright, Phys. Rev. B **57**, 2878 (1998).